RSC Advances

ROYAL SOCIETY OF CHEMISTRY

www.rsc.org/advances

Microstructure and corrosion behavior of Cr and Cr-P alloy coatings electrodeposited from a Cr(III)-deep eutectic solvent

Jialei Zhang[a,b], Changdong Gu*[a,b], Yueyu Tong[a,b], Junming Gou[a], Xiuli Wang[a,b], Jiangping Tu[a,b]

[a.]School of Materials Science and Engineering, State Key Laboratory of Silicon Materials, Zhejiang University, Hangzhou 310027, China

[b.]Key Laboratory of Advanced Materials and Applications for Batteries of Zhejiang Province, Hangzhou 310027, China

* Corresponding author. E-mail addresses: cdgu@zju.edu.cn; changdong_gu@hotmail.com; (C.D. Gu), Tel./fax: +86 571 87952573.

Abstract

Cr and Cr-P coatings were electrodeposited on Fe substrates from non-aqueous deep eutectic solvent-based electrolytes containing Cr(III). The optimized deposition parameters for the coating process were explored. A two-step process of Cr(III) reduction occurred, i.e. Cr(III)→Cr(II)→Cr(0), and the controlling step was promoted by adding $NH_4H_2PO_2$. It is found that an electro-brush plating Ni underlayer was essential to obtain a smooth and compact Cr or Cr-P coating on the Fe substrate. The structure and composition of the as-deposited coatings were thoroughly analyzed. The corrosion behavior of the Cr and Cr-P coatings is quite different in the 3.5 wt.% NaCl and 0.1 M H_2SO_4 solutions, respectively. The diplex effects of the layered structures and ion-selective components in the as-prepared Cr-based coatings are suggested to be responsible for the different corrosion mechanism in different corrosion medium.

Keywords： *Electrodeposition, Cr(III), Cr-P alloy, deep eutectic solvent, corrosion mechanism*

1. Introduction

Electrodeposited chromium has been extensively used in martial and industrial fields due to its irreplaceable wear and corrosion resistance.[1-7] Electrolytes containing hexavalent chromium, Cr(VI), have been predominated for over a century for plating chromium coatings.[4] However, with the growing environmental pressures and health considerations, the conventional Cr(VI) plating process has received legal restrictions for its intense toxicity and carcinogenicity.[7] Organizations around the world such as the "waste of electric and electronic equipment" (WEEE) in the European Union, the Environmental Protection Agency (EPA) in the United States, have already enacted legislation that banned Cr(VI) from industry.[4, 6, 8]

As a promising alternative to Cr(VI) in the electroplating process, Cr(III) has been received significant attentions in the past decades. The less toxic Cr(III) occurs in many foods and some dietary intake is essential to human health.[9] Development and improvement in environmental-friendly Cr(III) electroplating technology have became a hot research area in the 21st century. Nowadays, many problems have arisen in the burgeoning Cr(III) electroplating process. For instance, the electrochemical reduction mechanism of trivalent Cr remains unclear.[9, 10] It is difficult to improve the thickness of Cr from Cr(III) plating bath.[11] The intermediate Cr^{3+} is unstable and easily oxidized to Cr^{6+} near the anode during electroplating.[12] It is hard to search for a suitable complex agent or electrolyte solvent for Cr(III) electrodeposition, because it is almost impossible to deposit Cr coatings from a simple aqueous Cr(III) solution due to a very stable $[Cr(H_2O)_6]^{3+}$ complex.[13-15] Moreover, a considerable hydrogen evolution cannot be avoided during the reduction of Cr^{3+} to Cr^0.[14, 15]

Nevertheless, a lot of efforts in the previous Cr(III) aqueous plating research reveal that high-quality Cr coatings can be electrodeposited from electrolytes containing complex ions which are constituted by trivalent Cr and organic acid complexants possessing less than six atoms of carbon.[10, 16, 17] Inevitably, the final Cr coatings electrodeposited from these baths usually contain a high carbon content due to the reduction of organic acids.[18] Meanwhile, great attentions have also been attracted on the electrodeposition of Cr(III) from ionic liquids which have the nature of multicomponent ions and complex organic species to facilitate the coordination chemistry or proton transfer.[19, 20] In other words, ionic liquids themselves could provide organic complexing agents for Cr(III) electrodeposition. Most investigations for non-aqueous Cr(III) electrodeposition are mainly focused on 1-butyl-3-methylimidazolium ([BMIM]) based ionic liquids.[2, 21-25] As well, a few researchers reported that chromium has been successfully electrodeposited form a relative cheep choline chloride based deep eutectic solvent (DES).[8, 26-28] On the other hand, the co-deposition of chromium and phosphorous is seldom explored.[3, 13, 18, 29, 30] The addition of a metalloid phosphorous to chromium may trigger better corrosion resistance.[18, 30] The mainly challenges for electrodepositing Cr-P alloy are accompanied by the problems of Cr(III) electrodeposition as mentioned above.

In this work, we proposed a Cr(III) electroplating process using DES based electrolyte to produce Cr coatings on Fe substrate. Cr-P alloy coating was also co-electrodeposited by adding ammonium hypophosphite ($NH_4H_2PO_2$) as a phosphorus source. The as-prepared Cr and Cr-P coatings are mainly Cr-based compounds containing Cr, Cr_2O_3, and $Cr(OH)_3$. The inevitable oxides and hydroxides, which results from the additional crystalline hydrate and

the surface oxidation, greatly influence the corrosion behavior of the as-deposited Cr and Cr-P coatings in NaCl and H_2SO_4 aqueous solutions.

2. Experimental

All reagents were bought from Shanghai Chemical Company, China and directly used without further purification. DES was prepared by mixing choline chloride [$HOC_2H_4N(CH_3)_3^+$ Cl^-] (AR, 98%) with ethylene glycol [$(CH_2OH)_2$] (AR, 99%) by a 1:2 mole ratio and stirred at 80 °C until a homogeneous liquid formed. The electrolyte for trivalent chromium electroplating was obtained by dissolving 0.3 M $CrCl_3 \cdot 6H_2O$ (AR, 99%) and 0.2 M NaCl (AR, 99.5%) in the above DES. The electrolyte for Cr-P electrodeposition was further added 0.05 M $NH_4H_2PO_2$ (AR, 97%). NaCl herein acts as a conductive agent and its indispensability is discussed in the following section. The conductivities of the electrolytes were determined by a DDBJ-350 portable conductivity meter (Shanghai Leici) with temperature and conductivity probes (T-818-B-6F and DJS-1CF platinum black). Cyclic voltammetry (CV) was used to study the deposition mechanism of Cr(III), which was carried out in a three-electrode system (CH Instruments, Inc., China) consisting of a platinum working electrode (0.8 cm^2), a platinum counter electrode and a silver wire quasi-reference electrode at 55 °C, using a scan rate of 20 mV s^{-1}.

A Ni underlayer with a thickness of ~2 μm was prepared on the iron sheet (0.2 mm in thickness with Fe>98.576% and C<0.025%) from 0.5 M $NiCl_2$-DES electrolyte by electro-brush plating at 4 V as our previous work.[31] The Cr and Cr-P coatings were then direct-current electrodeposited on the Fe/Ni from the above electrolytes at a constant potential of -1.2 V in a three-electrode electrochemical workstation (CH Instruments, Inc.,

China). Graphite was used as anode and Ag wire was used as quasi-reference electrode. The electrolyte was kept at 55 ℃ on a magnetic stirrer with a stirring rate of 800 r/min during the electrodeposition. After deposition for 30 min the Fe/Ni/Cr and Fe/Ni/Cr-P deposits were sequentially rinsed with methanol and deionized water and then dried with flowing nitrogen.

The crystalline structure of the deposit was investigated by X-ray diffraction (XRD, XPert Pro-MPD with CuKα radiation, λ=0.15406 nm). The surface morphology was observed by a field emission scanning electron microscope (FE-SEM, Hitachi SU-70). The surface topography and roughness were measured by an atomic force microscopy (AFM, Nanosurf NaioAFM, Switzerland) in a contact mode. An energy dispersive X-ray spectrometer (EDS) was used for the qualitative elemental analysis of the Cr and Cr-P surface. X-ray photoelectron spectroscopy (XPS, AXIS UTLTRADLD) was further employed to analyze the chemical composition and state of the coatings using AlKα (monochromatic) radiation with E=1486.6 eV. All the core level spectra were referred to C 1s peak at 284.8 eV.

Potentiodynamic polarization measurements were carried out in the 3.5 wt.% NaCl and 0.1 M H_2SO_4 aqueous solutions at room temperature using a three-electrode cell (CH Instruments, Inc., China) with a platinum plate as counter electrode and a Ag/AgCl electrode as reference electrode. The specimens covered by polyimide coatings leaving an exposed area of ~1 cm^2 were used as working electrodes. Each specimen was immersed into the solutions for about 20 min to stabilize the open-circuit potential. The corrosion potential (E_{corr}) and corrosion current density (i_{corr}) were obtained by Tafel extrapolation method from the potentiodynamic polarization curves with a scan rate of 1 mV s^{-1}.

3. Results and discussion

3.1. Electrodeposition behavior of Cr(III)

Figure 1a shows the conductivity change as a function of temperature in the electrolytes with different compositions. High temperature results in an anabatic thermal motion and a katabatic dynamic viscosity thus promoting the migration of ions and the significant increase of conductivity.[32] The electrolyte of choline chloride-ethylene glycol dissolved by $CrCl_3$ exhibits a much higher conductivity than that of choline chloride mixed with $CrCl_3$.[26] Moreover, the addition of NaCl increases the conductivity, which should be due to the increase of the total ionic concentration in the electrolyte.[33] However, a conductivity decrease is found in the $CrCl_3$-electrolyte when further dissolving $NH_4H_2PO_2$, which indicates a complexation between $CrCl_3$ and $NH_4H_2PO_2$. Hereafter, NaCl is acquiescently added in the electrolytes for each measurement to increase the conductivity.

Figure 1b gives the CV curves of the DES-based electrolytes containing $CrCl_3$ and $CrCl_3$+$NH_4H_2PO_2$ at 55 °C. The potential scan started from 1.0 V (vs. Ag wire), in the negative potential direction up to -1.5 V, and then reversed to the starting potential at a scan rate of 20 mV s^{-1}.The $CrCl_3$-elctrolyte reveals two pairs of redox peaks, which agree with the two consecutive reduction steps of Cr(III) reduction, i.e. Cr(III)→Cr(II)→Cr(0).[8, 16, 34] In the cathodic branch, with increasing negative potential a reduction peak, A_c, is observed at about -0.75 V which is corresponding to the reduction of Cr(III) to Cr(II). At around -1.13 V the current density raises steeply (peak B_c), which may be attributed to the formation of metallic Cr along with the decomposition of electrolyte. Qualitatively, the onset potentials of reduction corresponding to Cr(III)/Cr(II) and Cr(II)/Cr(0) in the choline chloride-ethylene glycol DES are more positive than those in the choline chloride-chromium trichloride DES.[8,

[26] In the reverse scan, the anodic peaks of B_a and A_a are assigned to the oxidation of Cr(0) to Cr(II) and Cr(II) to Cr(III), respectively. In addition, the presence of a crossover occurred at about -1.0 V is the sign of a nucleation and growth process.[35] The addition of ammonium phosphite into the $CrCl_3$-electrolyte has a remarkable influence on the kinetics of the Cr(III) electrodeposition. The decreased current density agrees with the decrease in conductivity as shown in Figure 1a. In the cathodic branch, it is observed that the onset potential of Cr(III)/Cr(II) shifts from 0.00 V towards the negative region to -0.10 V while that of Cr(II)/Cr(0) shifts from -1.13 V towards the positive region to -0.95 V. These features indicate $NH_4H_2PO_2$ can inhibit the reduction process of Cr(III) to Cr(II), but promote the formation of Cr(0) from Cr(II). Accordingly, the anodic peak corresponding to Cr(II)/Cr(0) is positively shifted (-0.55 V to -0.46 V) while that corresponding to Cr(III)/Cr(II) is negatively shifted (0.14 V to -0.18 V), which suggests an inhibition of Cr(0) to Cr(II) and a promotion of Cr(II) to Cr(III). As a result, the range between cathodic peak and anodic peak is narrowed by adding $NH_4H_2PO_2$, which means the polarization is reduced. It has been reported that most Cr^{3+} complexes undergo stepwise charge transfer at the electrode in which the second step of Cr^{2+} reduction is slow.[29] Therefore, with the addition of $NH_4H_2PO_2$ the kinetics of Cr(III) electrodeposition is significantly enhanced. It is noted that the absence of the crossover for the $NH_4H_2PO_2$-added electrolyte during the negative and reverse scans results from the absence of nucleation and growth. This phenomenon is attributed to the formation of chromium hydroxides or chromium oxides occupying the sites of nucleation, thus blocking the Cr deposition on the surface of the electrode.[36]

A large number of experiments in this work reveal that the Cr(III) electrodeposition in this

system is very sensitive to the deposition parameters. Most of them are related to the deposition potential (controlling nucleation kinetics) and current density (controlling growth rate). Figure 1c shows the current-time curves during Cr(III) electrodeposition on Fe substrate using variable potentials at 55 °C with a stirring rate of 800 r/min. Three potentials of -1.1, -1.2 and -1.4 V (vs. Ag wire) were attempted for the Cr(III) deposition. No film was obtained at -1.1 V because it is a little more positive than -1.13 V and cannot lead to the reduction of Cr(II) to Cr(0), as discussed in Figure 1b. At the potential of -1.4 V, the film is pulverous and can be easily detached from the substrate under rinsing by water. Thus, the allowed deposition potentials for an acceptable chromium film are around -1.2 to -1.3 V. The current density was adjusted by adding NaCl or changing the temperature and stirring rate at -1.2 V. It was found that the cathodic current density range for chromium film formation is around 7 to 10 mA cm^{-2}. High-quality chromium cannot be electrodeposited at -1.2 V if the current density is incompetent. The addition of NaCl and applied stirring rate of 800 r/min and temperature of 55 °C are appropriate for obtaining the current density range for Cr and Cr-P deposition at -1.2 V.

3.2. Surface morphology and chemical composition of the coatings

Figure 2 reveals the SEM images of the electrodeposited Cr and Cr-P coatings on Fe and Fe/Ni substrates. The Fe/Cr coating electrodeposited at -1.4 V (vs. Ag wire) exhibits a nodular and creviced surface, as shown in Figure 2a. The cracks divided the coating into island-like structure with the island size of ~4 μm. The black particles are gathered by spheres and gently attached on the substrate, as shown in Figure 2b. Cracks can also be found in the deposits. The cracked and spalled morphology should result from the surface

pulverization of the deposits along with the electrochemical decomposition of the DES electrolyte at a high negative potential of -1.4 V. The decomposition products of choline chloride-ethylene glycol DES contain 88% hydrogen which could cause efflorescence of the deposits.[37] No nodules or cracks are found in the Fe/Cr coating deposited at -1.2 V. However, the substrate seems not to be fully covered. Although compact surface without any nodules or cracks is obtained in the local area, as shown in the inset of Figure 2c, some voids can be found in the Fe/Cr coating. When changing the substrate from Fe to electro-brush plated Ni, a uniform Fe/Ni/Cr coating is obtained which is very smooth and compact, as shown in Figure 2d. Spherical clusters with a size of ~200 nm and fine particles compose a crack-free surface. Similar morphologies are observed when depositing Cr-P coatings, as shown in Fig 2e and f. The Fe/Cr-P coating exhibits an uneven surface with voids while the Fe/Ni/Cr-P coating shows a glossy and dense surface with fine particles.

It is reported that thick Cr coatings cannot be readily obtained from Cr(III) electrolytes.[16] The as-deposited Cr and Cr-P coatings are very thin as well in this work, which have the average thicknesses of 700 nm and 500 nm, respectively. The surface morphology of the deposit therefore must be strongly influenced by the roughness of the substrate. Figure 3 depicts the typical three-dimensional AFM images (5 μm×5 μm) of the Fe/Ni, Fe/Cr, Fe/Ni/Cr and Fe/Ni/Cr-P coatings .The surface roughness of the electro-brush plated Ni is ~6 nm, as shown in Figure 3a, which is much smaller than the anode treated Fe substrate (~55 nm, not given here).[31] The Fe/Cr coating has a roughness of ~52 nm which is close to the Fe substrate. Deep voids can be observed in the Fe/Cr coating in Figure 3b and the defective surface is consistent with the SEM image in Figure 2c. Much smoother Cr and Cr-P coating

are deposited on the electro-brush plated Ni underlayer, and the roughnesses are measured to be ~12 nm and 8 nm, respectively. Large cluster and small particles can be observed in the Fe/Ni/Cr coating whereas only small particles can be found in the Fe/Ni/Cr-P coating. The morphology refinement of the Fe/Ni/Cr-P coating is correlated with the promotion of nucleation rate of Cr(II)→Cr(0) and inhibition of crystal growth rate by low current density when adding $NH_4H_2PO_2$, as discussed in the CV curves in Figure 1b. The surface morphology and roughness of the as-deposited Cr or Cr-P thin film greatly depend on the roughness of the substrate.

Figure 4 presents the EDS analyses of the electrodeposited Fe/Ni/Cr and Fe/Ni/Cr-P coatings. The EDS element mapping corresponding to the SEM image in Figure 2f is also given in this figure. Elements of C, O, Cl, Fe, Ni and Cr are detected on the surface of the Cr and Cr-P coatings, as shown in Figure 4a and b. The signals of carbon mainly come from the used conductive carbon tapes. However, the intensity of the EDS peak corresponding to oxygen is extremely strong which should not be only caused by the conductive carbon tapes. This result should be ascribed to the chromium oxides and/or hydroxides in the deposits.[9, 10] The impurity of chlorine in the deposits comes from the chromium chloride plating bath, which is detrimental to its pitting corrosion resistance.[3] About 6 at.% of phosphorus is detected in the Fe/Ni/Cr-P coating, as shown in Figure 4b. The introduction of phosphorus in the deposit results from the well-known induced deposition with the presence of an iron-group metal (Cr).[38] In consideration of no other reduction peaks observed in the CV curve in Figure 1b, the only reduced product consequently should be metallic Cr. In other words, the detected phosphorus is primarily in a form of oxides or elemental solute in the

Cr-based deposits. The elements of Cr and P hence have a uniform distribution in the Fe/Ni/Cr-P coating, as shown in Figure 4c and d.

3.3. Crystal structure and surface state of the coatings

The XRD patterns of the as-deposited Fe/Ni/Cr and Fe/Ni/Cr-P coatings are displayed in Figure 5. It is possible to detect that the compositions of the thin coatings possess weak peaks corresponding to Cr. The broaden peaks between 41.6° and 50.1° suggest a complicated compound with amorphous structure of the Cr-based coatings. It can be hardly found any differences between the Fe/Ni/Cr and Fe/Ni/Cr-P coatings because they are ultrathin.

For better understanding of the differences between the Fe/Ni/Cr and Fe/Ni/Cr-P coatings, XPS of the as-deposited coatings are further investigated, as shown in Figure 6. The binding energies (BEs) in the XPS spectra are calibrated by using that of C 1s (284.8 eV). The XPS survey spectra of the Cr and Cr-P coatings demonstrate that the elements are C, O, Cr, Cl and P (in the Cr-P coating), which agree well with the EDS analyses in Figure 4. As provided in Figure 6b, the Cr $2p_{3/2}$ peak can be resolved into three peaks that correspond to 574.1, 576.6 and 577.7 eV representing the Cr^0, Cr^{3+} in oxides and Cr^{3+} in hydroxides, respectively.[39-42] The inevitable oxides and hydroxides caused by the additional crystalline hydrate and the surface oxidation result in a partial presence of the metallic phase (Cr^0) in the deposits. No peaks around 586.7 eV are found demonstrating that Cr(VI) is not formed in the deposits. Chromium therefore exists in two different charge states in the as-prepared coatings. As for the Fe/Ni/Cr-P coating, a significant increase of peak area corresponding to Cr hydroxides, either in the form of $Cr(OH)_3$ or CrOOH, is obtained indicating a $Cr(OH)_3$

riched Cr-P coating. The increased ratio of $Cr(OH)_3/Cr_2O_3$ results in a distinct shift towards the high BE region of the Cr 2p peaks in the oxidized state as shown in Figure 6b. Besides, the Cr 2p peaks corresponding to Cr^0 remain at 574.1 and 583.4 eV. A similar compositive Cr $2p_{3/2}$ peak at 577.47 eV was detected by Li et al. when prepareing Cr-P coatings by electrodeposition from trivalent chromium electrolytes.[13] Tharamani et al. found the Cr $2p_{3/2}$ core level is higher and decreases on heat treatment at 673 K when preparing Cr-P coating by electroless plating from trivalent chromium electrolytes, which suggests a dehydration process of Cr hydroxides.[30] These shifts in BEs demonstrate the essential factor of Cr hydroxides in the Cr-P coatings prepared from trivalent chromium electrolytes with hypophosphite as a phosphorus source.

The P 2p core level spectrum for the Fe/Ni/Cr-P coating reveals three peaks at 129.1, 129.8 and 133.2 eV, as shown in Figure 6c. The BE at 129.8 eV is assigned to the elemental P and the other two BEs corresponds to its positively and negatively charged state, i.e. P^{5+} and $P^{\delta-}$.[13, 30] The $P^{\delta-}$ species at 129.1eV may come from the CrP_x formed on the surface,[18, 43] whereas the P^{5+} species at 129.8 eV should result from phosphate species and/or P_2O_5.[44]

3.4. Corrosion behavior of the coatings

Figure 7 reveals the potentiodynamic polarization curves for the Fe substrate, Fe/Ni, Fe/Ni/Cr and Fe/Ni/Cr-P coatings performed in the 3.5 wt.% NaCl and 0.1 M H_2SO_4 aqueous solutions at room temperature. The corresponding corrosion potential (E_{corr}) and corrosion current density (i_{corr}) are derived from the polarization curves (Figure 7) through Tafel extrapolation and summarized in Table 1. In the polarization curve, the cathodic branch is corresponding to the hydrogen evolution whereas the anodic branch has important

features related to the corrosion resistance of the coating or substrate. As shown in Figure 7a, the electro-brush plated Ni coating on Fe substrate (Fe/Ni) shows an enhanced corrosion resistance in NaCl solution as reported by our previous work.[31] After a 700 nm thick of Cr layer deposited on the Fe/Ni, the Fe/Ni/Cr coating exhibits the best corrosion resistance with the most positive E_{corr} of -437 mV (vs. Ag/AgCl) and lowest i_{corr} of 4.78 μA cm^{-2}. However, a worse corrosion resistance is obtained for the Fe/Ni/Cr-P coating with a Cr-P thickness of 500 nm, which is characterized by more negative E_{corr} and higher i_{corr} than Fe/Ni. No distinct passivation behaviors are found in the Cr and Cr-P coatings performed in NaCl solution, which implies pitting corrosion in the ultrathin coatings. However, a slower increase of current density in the anodic branch is observed in Cr or Cr-P coating performed in H_2SO_4 solution, as the buffer shown in Figure 7b. It must be caused by a weak passivation or inhibition of the Cr and Cr oxides/hydroxides in the as-deposited Cr/Cr-P coating. An increased i_{corr} is obtained for the Fe/Ni coating which is even higher than Fe substrate. This can be understood as there is no passivation occurred and more defect sites of grain boundaries in nanocrystalline Ni with a grain size of ~6 nm,[31] which increases the electrochemical reactivity and accelerates the corrosion of Ni.[45] The Fe/Ni/Cr-P coating possesses a better corrosion resistance with a more positive E_{corr} of -406 mV and lower i_{corr} of 0.121 mA cm^{-2} than those of the Fe/Ni/Cr coating.

The different corrosion performance for the Cr and Cr-P coatings in NaCl and H_2SO_4 solutions should result from different corrosion mechanism. The surface morphologies of the corroded films are therefore investigated as provided in Figure 8. Accordingly, two kinds of corrosion mechanism are schematically illustrated in Figure 9 to explain the different

corrosion behavior for the as-depostied Cr and Cr-P coatings in the 3.5 wt.% NaCl and 0.1 M H_2SO_4 solutions. Sheet-like corrosion products are tightly attached to the corroded Cr and Cr-P coatings and large cracks can be observed, as shown in Figure 8a and b. Although both the as-deposited Cr and Cr-P coating exhibit compact and crack-free surfaces, as shown in Figure 2d and f, defects such as internal stress and chlorine exist in the coatings. For example, the introduction of hydrate, $CrCl_3 \cdot 6H_2O$, provides at least 1.8 M H_2O which usually results in hydrogen into the deposits and causes internal stress and brittleness. These defects cause initial pitting and then evolve as following.

In NaCl solution (Figure 9a), the mainly aggressive ion Cl^- could cause serious pitting corrosion which occurred perpendicularly to the Cr or Cr-P coating along the initial pitting. According to the polarization curves in Fugure 7a, the E_{corr} of Ni is more negative than Cr but more positive than Cr-P, which means the priority for corrosion would be Cr-P>Ni>Cr in NaCl solution. Therefore, for the Cr coating, a lateral corrosion extends in the Ni underlayer and gases subsequently formed under the Cr coating. As internal stress remained in the upper brittle Cr layer, cracks forms near the initial pitting and delamination occurs along the cracks, as shown in Figure 8a. On the other hand, since the Cr coating is Cr_2O_3 riched, which is anion-selective,[46, 47] Cl^- can favorably permeate into the coating and also corrodes the Cr layer. The sheet-like particles hence formed on the Cr surface. However, the $Cr(OH)_3$ riched Fe/Ni/Cr-P coating is cation-selective,[48] and it can weaken Cl^- from directly going through, which results in more Cl^- migrating into the initial pitting and aggravating it. The pitting thereby is enlarged and collapsed near the cracks thus leading to a larger contact area of the Ni underlayer and the corrosive medium. Then the corrosion is accelerated as

characterized by higher current density in Figure 7a. Meanwhile, the Cr-P coating has a more negative E_{corr} than Ni and it is corroded prior to Ni, which leads to more corrosion products on the Cr-P surface, especially near the big pitting (enlarged from the initial pitting). As a result, larger and deeper pitting and more corrosion products on the surface are found in the Cr-P coating than that in the Cr coating. The Fe/Ni/Cr-P coating therefore shows a worse corrosion resistance in NaCl solution. Ramezani-Varzaneh et al. also mentioned that the addition of P from NaH_2PO_2 deteriorates anti-corrosion performance of the electrodeposited coatings in the 3.5 wt.% NaCl solution.[3] In the case of ultrathin amorphous Cr-P coating in this work, the defects introduced by P should significantly influence the corrosion performance.

As for the case of H_2SO_4 solution (Figure 9b), the mainly aggressive ion is H^+ and general uniform corrosions occurred. In this case, the initial pitting caused by defects would not be aggravated or enlarged so severely. As shown in Figure 8c and d, several deep pittings with a size of ~200 nm are found in the Cr coating while numerous shallow pittings with a size of 100-300 nm are observed on the Cr-P coating. These pittings should be originated from partial impurity of chlorine in the as-prepared coatings which is detected by EDS and XPS in Figure 4a, b and 6a. It has been reported that the chromium coating electrodeposited from chromium chloride exhibits a worse corrosion resistance than that from chromium sulfate and the electrolyte nature has a significant influence on the corrosion performance of chromium coatings.[3] Although Ni has a more negative E_{corr} than Cr in H_2SO_4 solution (see Fugure 7b), compared with the bare Fe/Ni few defect sites of Ni are exposed in the corrosive medium through a pitting with ~200 nm in diameter on the Cr surface. It means the active

Fe/Ni is well protected by a thin Cr/Cr-P coating in H_2SO_4 solution. On the other hand, the anion-selective Cr_2O_3 riched Fe/Ni/Cr coating inhibits H^+ from further corroding the coating and more H^+ migrate to the initial pitting, which result in a longitudinal corrosion and small deep pitting on the Cr coating. Furthermore, the cation-selective $Cr(OH)_3$ riched Fe/Ni/Cr-P coating acts as a buffer layer which leads to an increase of pH value and retards the permeated H^+ in the interface range.[49] Therefore, the Cr-P coating in comparison with the Cr coating has a better corrosion resistance in H_2SO_4 solution.

4. Conclusions

This work proposed a trivalent chromium electroplating process for Cr and Cr-P coatings from a choline chloride-ethylene glycol deep eutectic solvent. Cyclic voltammetry of the Cr(III)-electrolyte shows a conventional two-step process of Cr(III) reduction, i.e. Cr(III)→Cr(II)→Cr(0), and a promoted controlling step of the reaction by adding $NH_4H_2PO_2$. Cr(III) electrodeposition in this system is so sensitive that he deposition potential (or the cathodic current density) for a successful electrodeposition should be strictly maintained in the rage of -1.2 to -1.3 V vs. Ag wire (or 7 to 10 mA cm^{-2}). Smooth and compact Cr (700 nm thick) and Cr-P (500 nm thick) surfaces can be obtained on the electro-brush plated Ni underlayer on Fe substrates. The as-prepared Cr and Cr-P coatings are mainly Cr-based compounds containing Cr, Cr_2O_3, and $Cr(OH)_3$. Much higher $Cr(OH)_3$ content is detected in the Cr-P coating. Although crack-free chromium coatings are electrodeposited, defects such as internal stress and chlorine remain in the coatings, which result in cracks and pitting corrosion in the corrosive mediums. Different corrosion resistance between layers and ion selectivity of Cr_2O_3 and $Cr(OH)_3$ result in a worse

anti-corrosion performance of Cr-P coating in NaCl solution but a better one in H_2SO_4 solution.

Acknowledgments

This work was supported by the National Natural Science Foundation of China (51271169) and the Key Science and Technology Innovation Team of Zhejiang Province under grant number 2010R50013.

References

1. A. Liang, L. Ni, Q. Liu and J. Zhang, *Surf. Coat. Technol.*, 2013, **218**, 23.
2. X. He, Q. Zhu, B. Hou, C. Li, Y. Jiang, C. Zhang and L. Wu, *Surf. Coat. Technol.*, 2015, **262**, 148.
3. H. Ramezani-Varzaneh, S. Allahkaram and M. Isakhani-Zakaria, *Surf. Coat. Technol.*, 2014, **244**, 158.
4. Z. Zeng, L. Wang, A. Liang and J. Zhang, *Electrochim. Acta*, 2006, **52**, 1366.
5. C. E. Lu, N. W. Pu, K. H. Hou, C. C. Tseng and M. D. Ger, *Appl. Surf. Sci.*, 2013, **282**, 544.
6. G. Saravanan and S. Mohan, *Corros. Sci.*, 2009, **51**, 197.
7. G. Hong, K. Siow, G. Zhiqiang and A. Hsieh, *Plat. surf. finish.*, 2001, **88**, 69.
8. E. S. Ferreira, C. Pereira and A. Silva, *J. Electroanal. Chem.*, 2013, **707**, 52.
9. Z. A. Hamid, *Surf. Coat. Technol.*, 2009, **203**, 3442.
10. Z. Zeng, Y. Sun and J. Zhang, *Electrochem. Commun.*, 2009, **11**, 331.
11. Y. B. Song and D. T. Chin, *Plat. surf. finish.*, 2000, **87**, 80.
12. J. McDougall, M. El-Sharif and S. Ma, *J. Appl. Electrochem.*, 1998, **28**, 929.
13. B. Li, A. Lin and F. Gan, *Surf. Coat. Technol.*, 2006, **201**, 2578.
14. R. Giovanardi and G. Orlando, *Surf. Coat. Technol.*, 2011, **205**, 3947.
15. R. Giovanardi and A. Bozza, *Metall. Ital.*, 2014, 9.
16. Y. Song and D. T. Chin, *Electrochim. Acta*, 2002, **48**, 349.
17. G. Saravanan and S. Mohan, *J. Appl. Electrochem.*, 2010, **40**, 1.
18. Z. Zeng, A. Liang and J. Zhang, *Electrochim. Acta*, 2008, **53**, 7344.

19. J. L. Zhang, C. D. Gu, Y. Y. Tong, X. L. Wang and J. P. Tu, *J. Electrochem. Soc.*, 2015, **162**, D313.

20. J. M. Rimsza and L. R. Corrales, *Comput. Theor. Chem.*, 2012, **987**, 57.

21. S. Eugenio, C. Rangel, R. Vilar and S. Quaresma, *Electrochim. Acta*, 2011, **56**, 10347.

22. S. Survilienė, S. Eugenio and R. Vilar, *J. Appl. Electrochem.*, 2011, **41**, 107.

23. S. Eugenio, C. M. Rangel, R. Vilar and A. M. B. do Rego, *Thin Solid Films*, 2011, **519**, 1845.

24. X. K. He, B. L. Hou, C. Li, Q. Y. Zhu, Y. M. Jiang and L. Y. Wu, *Electrochim. Acta*, 2014, **130**, 245.

25. Y. Hasimu, R. Q. Liu and H. Y. Mi, *Chem. J. Chin. Univ.-Chin.*, 2014, **35**, 140.

26. A. P. Abbott, G. Capper, D. L. Davies, R. K. Rasheed, J. Archer and C. John, *Trans. Inst. Met. Finish.*, 2004, **82**, 14.

27. Y. Lin, Y. Cui and Y. X. Hua, *Res. J. Chem. Environ.*, 2012, **16**, 116.

28. D. McCalman, L. Sun, Y. Zhang, E. J. Maginn, J. F. Brennecke and W. F. Schneider, *J. Phys. Chem. B*, 2015.

29. C. Tharamani, V. Murulidharan and S. Mayanna, *Int. J. Electrochem. Sci.*, 2007, **2**, 734.

30. C. Tharamani, F. S. Hoor, N. S. Begum and S. Mayanna, *J. Solid State Electrochem.*, 2005, **9**, 476.

31. C. D. Gu, J. L. Zhang, W. Q. Bai, Y. Y. Tong, X. L. Wang and J. P. Tu, *J. Electrochem. Soc.*, 2015, **162**, D159.

32. O. Ciocirlan, O. Iulian and O. Croitoru, *Rev. Chim.*, 2010, **61**, 7213.

33. J. Zhang, C. Gu, S. Fashu, Y. Tong, M. Huang, X. Wang and J. Tu, *J. Electrochem. Soc.*, 2015, **162**, D1.

34. S. Surviliene, A. Cešuniene, A. Selskis and R. Butkiene, *Trans. IMF*, 2013, **91**, 24.

35. F. R. Bento and L. H. Mascaro, *Surf. Coat. Technol.*, 2006, **201**, 1752.

36. Y. Messaoudi, N. Fenineche, A. Guittoum, A. Azizi, G. Schmerber and A. Dinia, *J. Mater. Sci.: Mater. Electron.*, 2013, **24**, 2962.

37. K. Haerens, E. Matthijs, K. Binnemans and B. Van der Bruggen, *Green Chem.*, 2009, **11**, 1357.

38. A. Brenner, *Electrodeposition of alloys: principles and practice*, Elsevier, 2013.

39. C. Anandan, V. W. Grips, K. Rajam, V. Jayaram and P. Bera, *Appl. Surf. Sci.*, 2002, **191**, 254.

40. M. Aguilar, E. Barrera, M. Palomar-Pardavé, L. Huerta and S. Muhl, *J. Non-Cryst. Solids*, 2003, **329**, 31.

41. V. Maurice, S. Cadot and P. Marcus, *Surf. Sci.*, 2001, **471**, 43.

42. X. Zhang, C. Van den Bos, W. Sloof, A. Hovestad, H. Terryn and J. De Wit, *Surf. Coat. Technol.*, 2005, **199**, 92.

43. P. E. Blanchard, A. P. Grosvenor, R. G. Cavell and A. Mar, *Chem. Mater.*, 2008, **20**, 7081.

44. M. Pelavin, D. Hendrickson, J. Hollander and W. Jolly, *J. Phys. Chem.*, 1970, **74**, 1116.

45. L. Y. Qin, J. S. Lian and Q. Jiang, *Trans. Nonferr. Met. Soc. China*, 2010, **20**, 82.

46. H. Yu, C. Chen, R. Jiang, P. Qiu and Y. Li, *J. Phys. Chem. C*, 2012, **116**, 25478.

47. B. Malki, O. Le Bacq, A. Pasturel and B. Baroux, *J. Electrochem. Soc.*, 2014, **161**, C486.

48. C. Chen, M. Lu, D. Sun, Z. Zhang and W. Chang, *Corrosion*, 2005, **61**, 594.

49. W. K. Chen, C. Y. Bai, C. M. Liu, C. S. Lin and M. D. Ger, *Appl. Surf. Sci.*, 2010, **256**, 4924.

Figure captions

Figure 1. (a) The conductivity change as a function of temperature in the electrolytes with different composition. (b) CV curves of the DES-based electrolytes containing $CrCl_3$ and $CrCl_3$+$NH_4H_2PO_2$. The scan rate is 20 mV s^{-1} (vs. Ag wire) and the temperature is 55 °C. (c) Current-time curves during Cr(III) electrodeposition on Fe substrate using variable potentials at 55 °C with a stirring rate of 800 r/min.

Figure 2. SEM images of the electrodeposited Cr and Cr-P coatings on Fe and Fe/Ni substrates. (a) Fe/Cr coating at -1.4 V, (b) Fe/Cr black particles at -1.4 V, (c) Fe/Cr coating at -1.2 V, (d) Fe/Ni/Cr coating at -1.2 V, (e) Fe/Cr-P coating at -1.2 V, (f) Fe/Ni/Cr-P coating at -1.2 V. All the potentials are referenced to the Ag wire.

Figure 3. Typical three-dimensional AFM images (5 μm×5 μm) of the Fe/Ni (a), Fe/Cr (b), Fe/Ni/Cr (c) and Fe/Ni/Cr-P (d) coatings. The roughness for each coating is also given.

Figure 4. EDS analyses of the electrodeposited Fe/Ni/Cr (a) and Fe/Ni/Cr-P (b) coatings. (c-d) EDS element mapping corresponding to the SEM image in Figure 2f of the Fe/Ni/Cr-P coating.

Figure 5. XRD patterns of the as-deposited Fe/Ni/Cr and Fe/Ni/Cr-P coatings. The reported PDF cards for Cr, Ni and Fe are also given in this figure.

Figure 6. (a) XPS survey spectra of the as-deposited Fe/Ni/Cr and Fe/Ni/Cr-P coatings (b-c) Cr 2p and P 2p XPS core-level spectra of the as-deposited coatings.

Figure 7. Potentiodynamic polarization curves for the Fe substrate, Fe/Ni, Fe/Ni/Cr and Fe/Ni/Cr-P coatings performed in the 3.5 wt.% NaCl (a) and 0.1 M H_2SO_4 (b)

aqueous solutions at room temperature.

Figure 8. Typical SEM images of the Cr and Cr-P coatings after corrosion measurements. (a) Fe/Ni/Cr in 3.5 wt.% NaCl, (b) Fe/Ni/Cr-P in 3.5 wt.% NaCl, (c) Fe/Ni/Cr in 0.1 M H_2SO_4, Fe/Ni/Cr-P in 0.1 M H_2SO_4.

Figure 9. Schematic illustrations of the corrosion mechanism for the as-deposited Fe/Ni/Cr and Fe/Ni/Cr-P coatings performed in the 3.5 wt.% NaCl (a) and 0.1 M H_2SO_4 (b) solutions.

Table caption

Table 1. Corrosion parameters of the Fe substrate, Fe/Ni, Fe/Ni/Cr and Fe/Ni/Cr-P coatings summarized from Figure 7a and b. The potentials are referenced to the Ag/AgCl electrode.

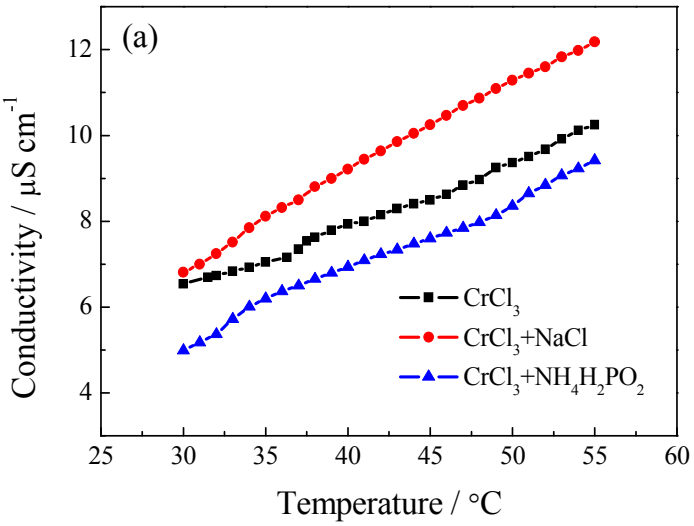

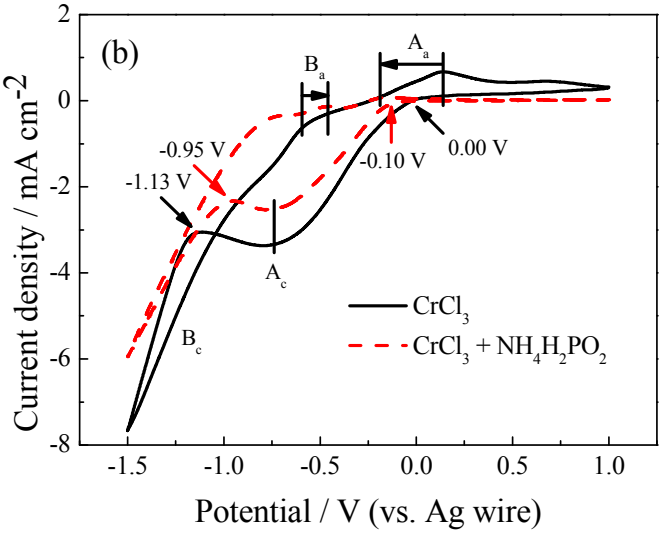

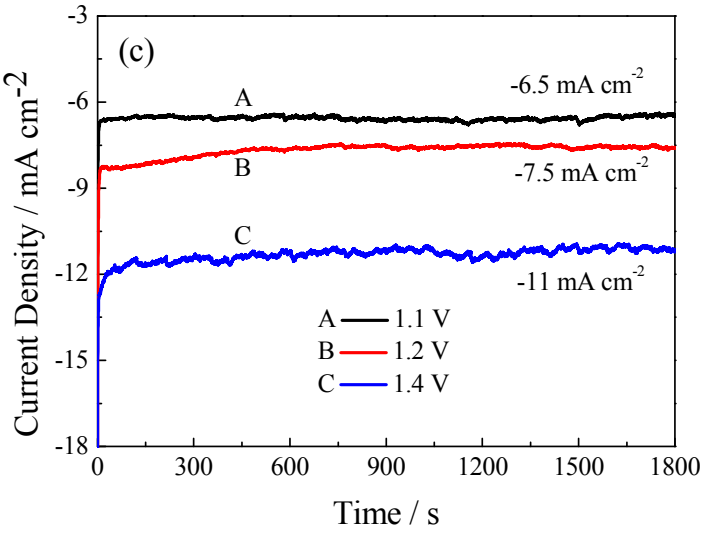

Figure 1.

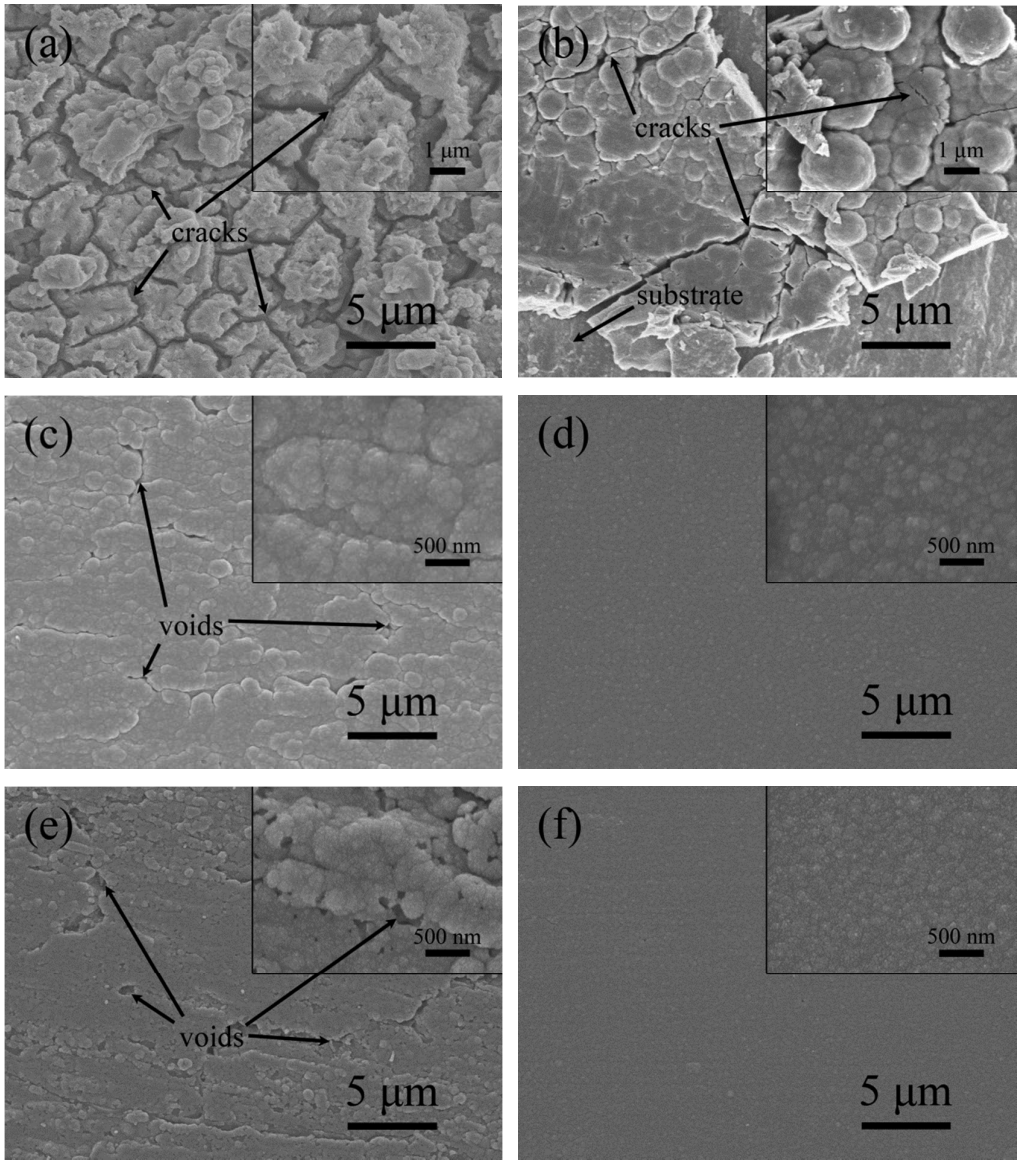

Figure 2.

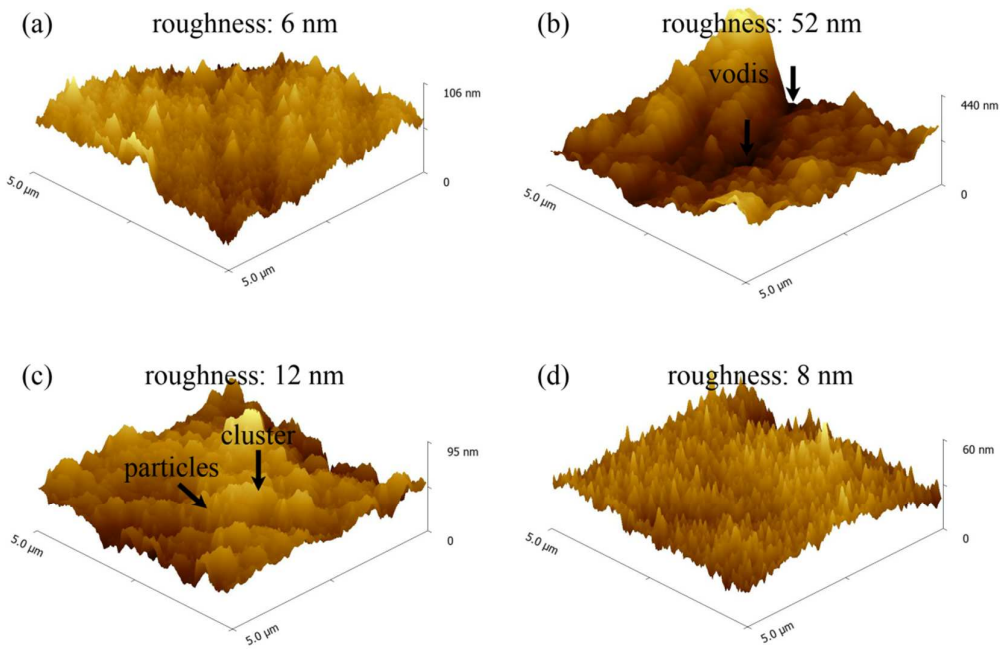

Figure 3.

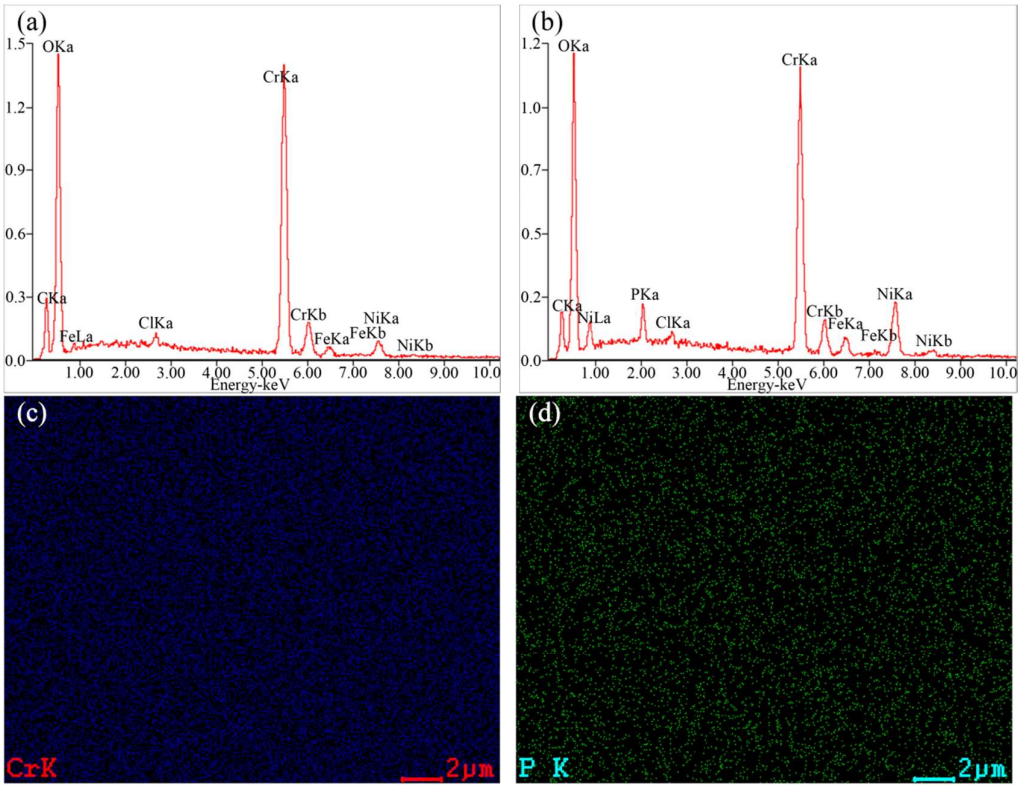

Figure 4.

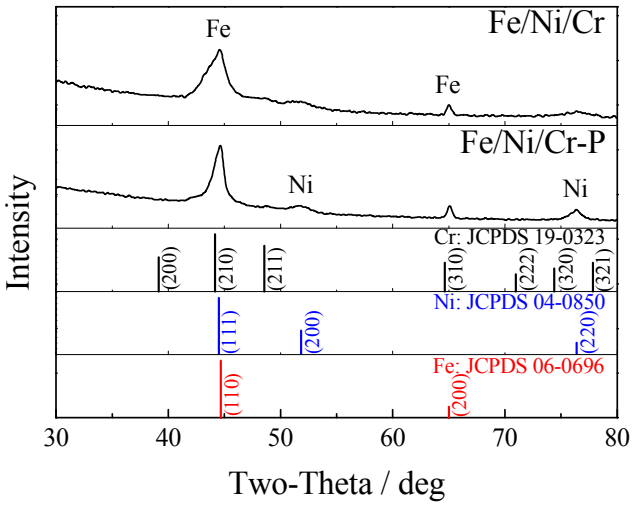

Figure 5.

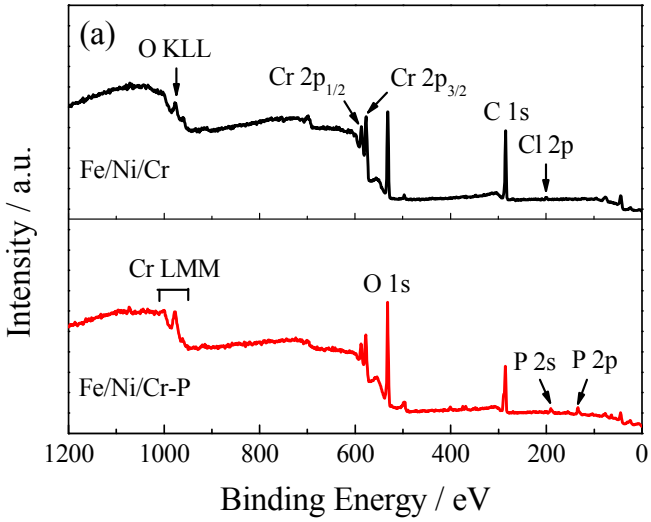

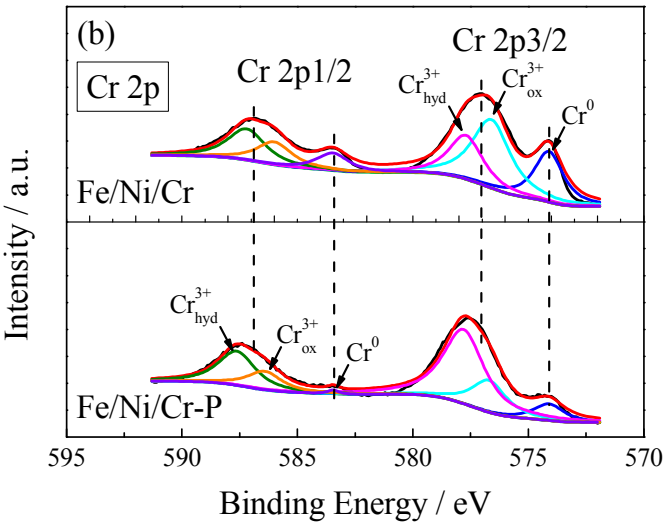

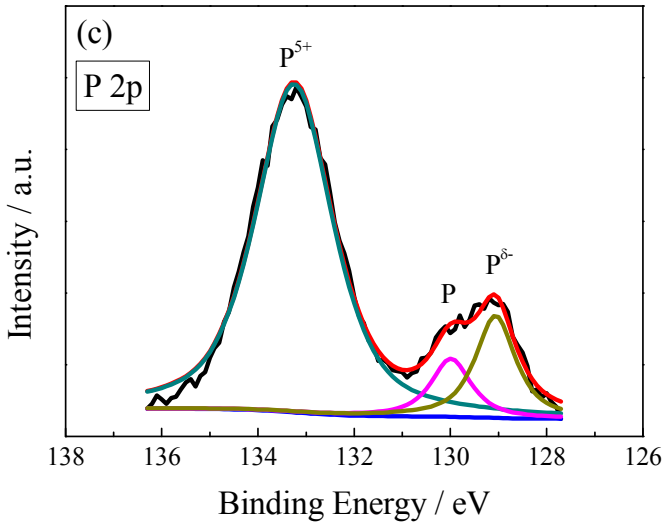

Figure 6.

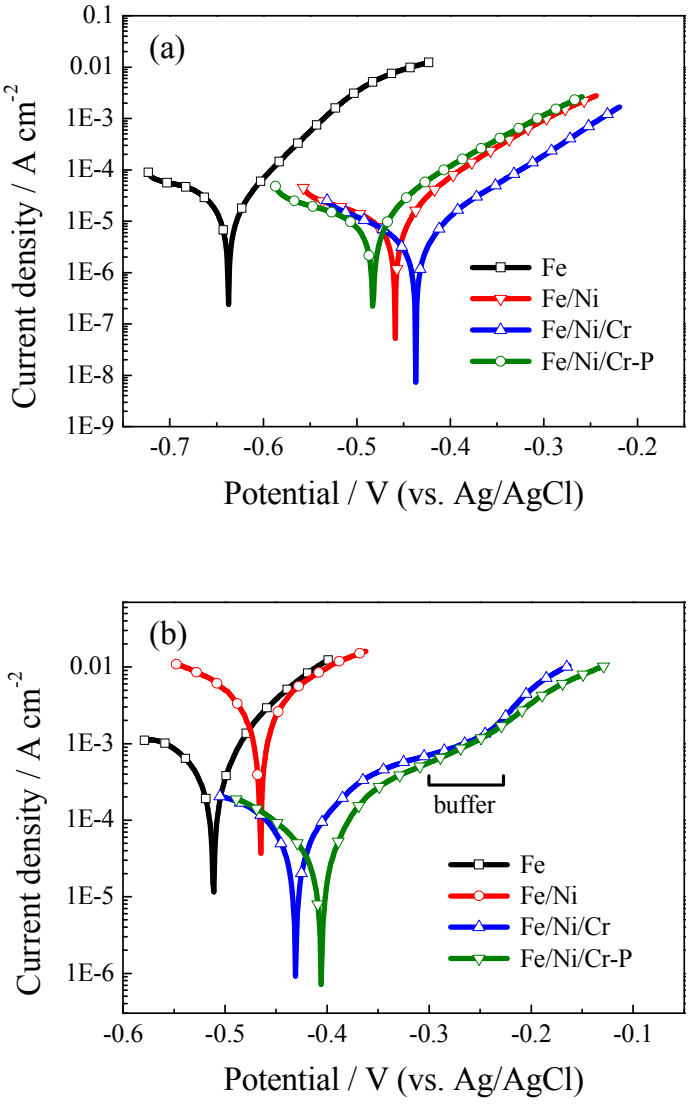

Figure 7.

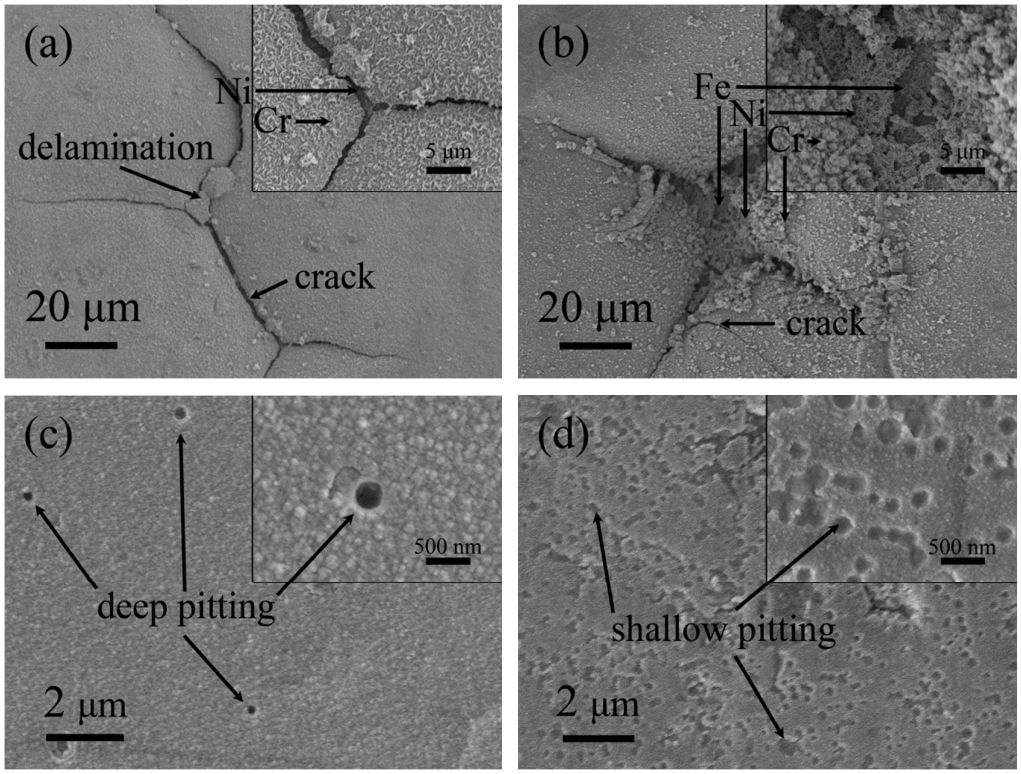

Figure 8.

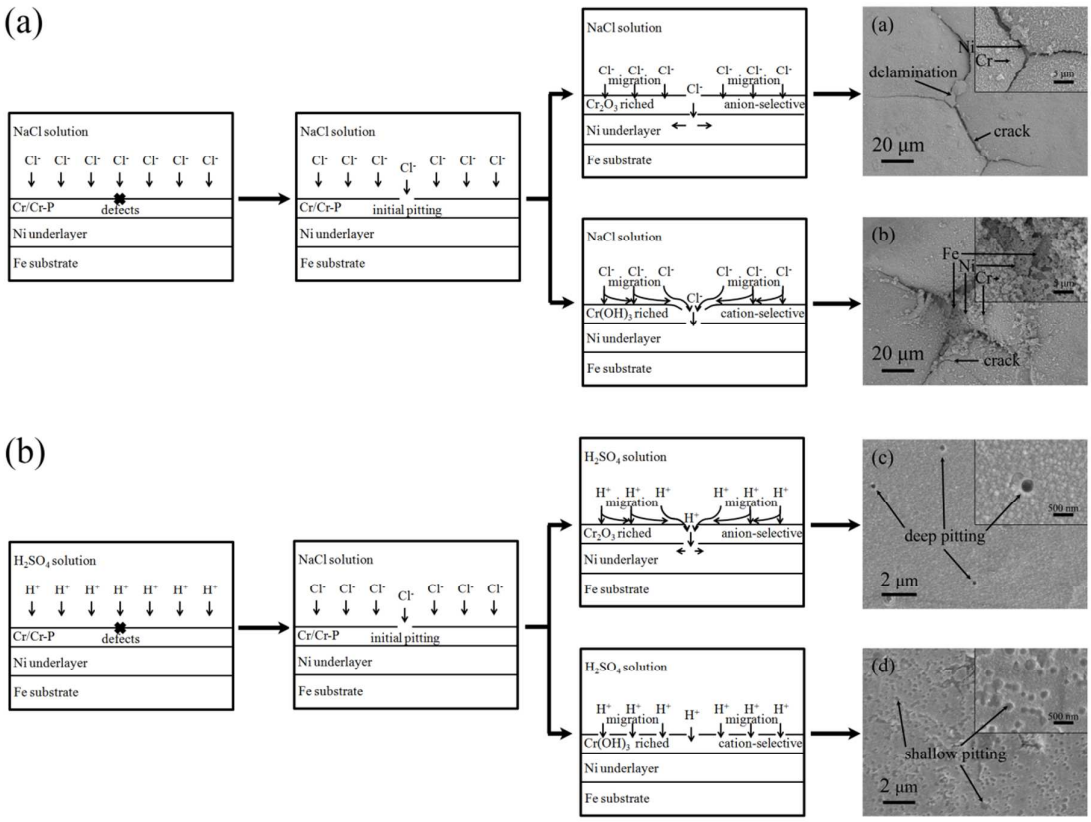

Figure 9.

Table 1.

Sample	E_{corr} (mV vs. Ag/AgCl) NaCl	i_{corr} (μA cm^{-2}) NaCl	E_{corr} (mV vs. Ag/AgCl) H_2SO_4	i_{corr} (mA cm^{-2}) H_2SO_4
Fe	-637	20.1	-511	1.06
Fe/Ni	-458	14.5	-465	4.45
Fe/Ni/Cr	-437	4.78	-431	0.177
Fe/Ni/Cr-P	-482	13.8	-406	0.121